The Canadian Mineralogist
Vol. 53, pp. 325-344 (2015)
DOI: 10.3749/canmin.1400084

FLUORCHEGEMITE, $Ca_7(SiO_4)_3F_2$, A NEW MINERAL FROM THE EDGREWITE-BEARING ENDOSKARN ZONE OF AN ALTERED XENOLITH IN IGNIMBRITES FROM UPPER CHEGEM CALDERA, NORTHERN CAUCASUS, KABARDINO-BALKARIA, RUSSIA: OCCURRENCE, CRYSTAL STRUCTURE, AND NEW DATA ON THE MINERAL ASSEMBLAGES

IRINA O. GALUSKINA[§]

Faculty of Earth Sciences, Department of Geochemistry, Mineralogy and Petrography, University of Silesia, Będzińska 60, 41-200 Sosnowiec, Poland

BILJANA KRÜGER[*]

Mineralogical Crystallography, Institute of Geological Sciences, University of Bern, Freiestrasse 3, CH-3012 Bern, Switzerland

EVGENY V. GALUSKIN

Faculty of Earth Sciences, Department of Geochemistry, Mineralogy and Petrography, University of Silesia, Będzińska 60, 41-200 Sosnowiec, Poland

THOMAS ARMBRUSTER

Mineralogical Crystallography, Institute of Geological Sciences, University of Bern, Freiestrasse 3, CH-3012 Bern, Switzerland

VIKTOR M. GAZEEV

Institute of Geology of Ore Deposits, Petrography, Mineralogy and Geochemistry (IGEM) RAS, Staromonetny 35, Moscow, Russia

ROMAN WŁODYKA

Faculty of Earth Sciences, Department of Geochemistry, Mineralogy and Petrography, University of Silesia, Będzińska 60, 41-200 Sosnowiec, Poland

MATEUSZ DULSKI

Institute of Physics, University of Silesia, Uniwersytecka 4, 40-007 Katowice, Poland

PIOTR DZIERŻANOWSKI

Institute of Geochemistry, Mineralogy and Petrology, Warsaw University, al. Żwirki i Wigury 93, 02-089 Warszawa, Poland

ABSTRACT

Fluorchegemite, $Ca_7(SiO_4)_3F_2$ [*Pbnm*, *a* 5.0620(1), *b* 11.3917(2), *c* 23.5180(3) Å, *V* 1356.16(4) Å^3, *Z* = 4], the F-analog of chegemite, $Ca_7(SiO_4)_3(OH)_2$ [*Pbnm*, *a* 5.0696(1), *b* 11.3955(1), *c* 23.5571(3) Å, *V* 1360.91(4) Å^3, *Z* = 4], was found in an edgrewite-bearing zone of endoskarn at the contact of a large altered calciferous xenolith within ignimbrites of the Upper Chegem Caldera, Northern Caucasus, Kabardino-Balkaria, Russia. Fluorchegemite is associated with the high-temperature minerals larnite, edgrewite, wadalite, eltyubyuite, rondorfite, lakargiite, Th-rich kerimasite, and with their alteration products such as bultfonteinite, killalaite, hillebrandite,

[§] *Corresponding author e-mail address*: irina.galuskina@us.edu.pl

[*] née Lazic, at present Institute of Mineralogy and Petrography, University of Innsbruck, Innrain 52, 6020 Innsbruck, Austria

afwillite, trabzonite, and jennite. Fluorchegemite is colorless, and the streak is white. It forms irregular grains up to 0.2 mm. Fluorchegemite gave the following optical data: biaxial (–), α 1.610(2), β 1.6150(2), γ 1.619(2) (589 nm), $2V_z$ (meas.) = 80(8)°, $2V_z$ (calc.) = 84°, Δ = 0.009, dispersion r > v, weak; non-pleochroic. Density (calc.) = 2.91 g cm^{-3}. The micro-hardness VHN (loaded 50 g) ranges between 480 and 511 kg mm^{-2}, with an average value (mean of four measurements) of 499(10) kg mm^{-2}, corresponding to a Mohs hardness of 5.5–6. The main bands in the Raman spectrum of fluorchegemite are at 258, 297, 410, 422, 560, 817, 843, 922, 3539, 3548, and 3552 cm^{-1}. Strong lines of the calculated X-ray diffraction pattern are [*d* (*hkl*)*I*]: 2.531(200)100, 1.905(227)90, 2.718(117)63, 3.013(131)57, 2.991(116)56, 3.636(114)52, 2.832(133)51, 2.699(134)46. The empirical formula of fluorchegemite from the holotype specimen is $(Ca_{7.01}Mg_{0.01})_{\Sigma 7.02}(Si_{2.98}Ti^{4+}_{0.01})_{\Sigma 2.99}O_{12}[F_{1.40}(OH)_{0.60}]_{\Sigma 2.00}$.

The Ca-humite minerals often form lens-shaped aggregates within the endoskarn zone. The elongated axis of the lens is oriented subperpendicular to the front of metasomatic replacement (skarn zonality). Lens-shaped aggregates of grains are interpreted as contours of replaced quartz phenocrysts in the ignimbrite. The mechanism of this lens formation is discussed. Moreover, lens-shaped aggregates of hydroxyledgrewite occur as rock-forming minerals in an endoskarn zone of a newly discovered xenolith within the Upper Chegem Caldera. In addition, the second finding of the Ca-humite minerals fluorchegemite and kumtyubeite, in an altered xenolith of the Shadil-Khokh volcano, Southern Ossetia, is reported.

Keywords: fluorchegemite, humite, edgrewite, structure, new mineral, Raman, skarn, Upper Chegem Caldera, Russia.

Introduction

Fluorchegemite, $Ca_7(SiO_4)_3F_2$ [*Pbnm*, *a* 5.0620(1), *b* 11.3917(2), *c* 23.5180(3) Å, *V* 1356.16(4) Å^3, *Z* = 4], the Ca-analog of humite, $Mg_7(SiO_4)_3F_2$, and F-analog of chegemite, $Ca_7(SiO_4)_3(OH)_2$, was found in an edgrewite-bearing zone of endoskarn at the contact of the largest of 11 known altered silicate-carbonate xenoliths (xenolith no. 1, about 20 m in diameter; Figs. 1, 2) within ignimbrites of the Upper Chegem Caldera, Northern Caucasus, Kabardino-Balkaria, Russia.

The Ca-humite series, belonging to the humite group, combines minerals with modular structures and the common crystal chemical formula $n{\cdot}Ca_2SiO_4 + Ca_3(SiO_4)(F,OH)_2$ (Thompson 1978, Galuskin *et al.* 2012a), where Ca_2SiO_4 represents a "calcio-olivine module" and $Ca_3(SiO_4)(F,OH)_2$ may be termed as "Ca-norbergite module". There are six known F- and OH-dominant Ca-humite minerals with n = 1, 2, 3. The member with n = 1 corresponds to the kumtyubeite $Ca_5(SiO_4)_2F_2$ – reinhardbraunsite $Ca_5(SiO_4)_2(OH)_2$ series, isostructural with chondrodite (Hamm & Hentschel 1983, Kirfel *et al.* 1983, Galuskina *et al.* 2009). The member with n = 2 corresponds to the chegemite $Ca_7(SiO_4)_3(OH)_2$ – fluorchegemite $Ca_7(SiO_4)_3F_2$ series, isostructural with humite (Galuskin *et al.* 2009). The member with n = 3 represents the edgrewite $Ca_9(SiO_4)_4F_2$ – hydroxyledgrewite $Ca_9(SiO_4)_4(OH)_2$ series, isostructural with clinohumite (Galuskin *et al.* 2012a). Minerals with n = 0 are absent in the polysomatic series of naturally occurring Ca- and Mn-humite minerals, but only occur in the Mg-humite series as the mineral norbergite $Mg_3SiO_4(F,OH)_2$ (Deer *et al.* 1978, Ribbe 1982).

Minerals of the reinhardbraunsite-kumtyubeite series have been reported from cement materials (Kantautas *et al.* 2006, Taylor 1997) and from burnt coal dumps (Sharygin 2011, Hršelová *et al.* 2013). Synthetic analogs of kumtyubeite and fluorchegemite are applied as luminescence matrices (Suresh *et al.* 2012).

In xenoliths embedded in ignimbrites of the Upper Chegem Caldera, between Lakargi and Vorlan peaks, all hitherto known Ca-humite minerals have been found. These xenoliths are the type localities for five mineral species, excluding only reinhardbraunsite (Galuskina *et al.* 2009, Galuskin *et al.* 2009, 2012a).

In the present paper we give a description of the new mineral species fluorchegemite (IMA2011-112), approved in 2012 by CNMNC IMA. The holotype specimen is deposited in the collection of the Fersman Mineralogical Museum (Moscow, Russia), catalog no. 4163/1. We also present data on kerimasite, associated with fluorchegemite, having the highest thorium content so far detected among minerals of the garnet supergroup. A formation mechanism for lens-shaped aggregates of Ca-humite minerals, elongated sub-perpendicular to the metasomatic front (skarn zonality), is proposed. Finally, a second finding of fluorchegemite and kumtyubeite from an altered xenolith of the Shadil-Khokh volcano, Southern Ossetia, is reported.

Experimental Details

Morphology and composition of the described minerals were determined using a Philips XL30/EDAX scanning electron microscope (Department of Earth Sciences, University of Silesia, Poland) and a CAMECA SX100 electron microprobe (Institute of Geochemistry, Mineralogy and Petrology, University of Warsaw, Poland). The following lines and standards were used for analyses of Ca-humite minerals (15 kV, 10–20 nA, 1–3 μm beam diameter): Ca*K*α, Si*K*α – wollastonite; Fe*K*α – hematite; Ti*K*α – rutile; Mn*K*α – rhodochrosite; Mg*K*α – diopside; Na*K*α – albite; Al*K*α – orthoclase; F*K*α – fluorophlogopite; Cl*K*α – tugtupite. Electron-microprobe compositions of Th-rich kerimasite were obtained at 15 kV and 40 nA using the following lines and standards: Al*K*α – orthoclase, Si*K*α – zircon, Ca*K*α – wollastonite, Sc*K*α – Sc, Ti*K*α – rutile, Fe*K*α – Fe_2O_3, Zr*L*α – zircon, Nb*L*α – Nb, Sn*L*α – cassiterite, Sb*L*α – Sb_2S_3, La*L*α – LaB_6, Ce*L*α – CeP_5O_{14}, Hf*M*α – Hf, Th*M*α – ThO_2, U*M*β – vorlanite.

The Raman investigations were performed using a WITec confocal CRM alpha 300 Raman microscope (Institute of Physics, University of Silesia, Poland). The spectrometer was equipped with an air-cooled solid-state laser operating at 532 nm and a CCD detector, which was cooled to –58 °C. The laser was coupled to the microscope *via* a single mode optical fiber with a diameter of 50 μm. The scattered radiation was focused onto a multi-mode fiber (50 μm diameter) and a monochromator. A dry Olympus MPLAN (50×/0.76NA or 100×/0.5NA) objective was used. Some 15–20 scans with integration times of 10–15 s and a resolution of 3 cm^{-1} were collected and averaged. The monochromator of the spectrometer was calibrated using the Raman scattering line produced by a silicon plate (520.7 cm^{-1}).

Reflectance infrared spectra were measured using a Bio-Rad FTS-6000 spectrophotometer equipped with a Bio-Rad UMA-500 infrared microscope (Institute of Physics, University of Silesia, Poland). The microscope had its own 250 × 250 mm mercury cadmium telluride detector (MTC) cooled to 77 K using liquid nitrogen. Spectra were obtained in the range 6000–700 cm^{-1} with a resolution of 4 cm^{-1}. Interferograms were recorded by accumulating 512 scans and a gold-covered microscope slide was used to obtain the background spectrum. IR radiation reflected by a polished grain of edgrewite (40 × 160 mm in thin-section) was collected. The reflection data were converted to a standard absorption spectrum using the Fourier and Kramers-Krönig transformation.

Single-crystal X-ray data for fluorchegemite were collected with a Bruker APEX II SMART diffractometer (Mo*K*α, λ = 0.71073 Å) (University of Bern, Switzerland). The structure was solved by direct methods, with subsequent analyses of difference-Fourier maps, and refined with neutral atom scattering factors using SHELXL (Sheldrick 2008).

Occurence and Description of Fluorchegemite

The Upper Chegem Caldera, extending about 100 km^2, is located in the eastern part of the Elbrus-Kyugen volcanic region (Bogatikov *et al.* 1992). At the lower part of the volcanic sequence, north-east of the Caldera, a granodiorite-porphyry stock (Figs. 1, 2) has intruded into a 1.5 km thick series of rhyolite-rhyodacite ignimbrites and tuffs. Higher in the geological succession, a two-pyroxene andesite lava overlies moraines of the Mindelian glacial stage. The age of the ignimbrites is 2.8–3.0 Ma, whereas the age of the younger granodiorite-porphyry is estimated to be 2.5 ± 0.2 Ma (Borsuk 1979) or 2.78 Ma (Lipman *et al.* 1993, Gazis *et al.* 1995). Persilicic ignimbrites of the Upper Chegem Caldera contain several small xenoliths (up to 5–7 cm in size) belonging to different lithologies, *i.e.*, Riphean and Lower Paleozoic crystalline schist, Late Paleozoic granites, Middle Jurassic sandstones, siltstones, and argillites, as well as Late Jurassic limestones (Bogatikov *et al.* 1992). Usually, the xenoliths are slightly altered. In marginal zones of carbonate xenoliths diopside and grossular-andradite, and more rarely wollastonite, have been identified, whereas the core of the xenoliths is composed of recrystallized calcite (marble). The large xenoliths (1–20 m in size) within ignimbrites of the Upper Chegem Caldera composed of altered carbonate-silicate rocks are exceptional. These xenoliths were metamorphosed up to sanidinite facies (larnite subfacies) (Gazeev *et al.* 2006, Galuskin *et al.* 2009) and are considered to be pyrometamorphic rocks, formed at very high temperature and very low pressure (Grapes 2011). There are three main occurrences of natural pyrometamorphic rocks: (1) altered xenoliths of carbonate-silicate rocks embedded in volcanites; (2) sedimentary rocks altered at high-temperature at contacts with magmatic basic rocks; and (3) baked and fused rocks resulting from combustion of organic material or gases. All three rock types have been sources of new minerals (*i.e.*, Galuskin *et al.* 2008, 2011a and b, 2012a, 2014, Lazic *et al.* 2011, Galuskina *et al.* 2010a and b, 2014a).

Over the last five years, more than 20 new mineral species have been discovered in the large altered xenoliths (at present there are 11 known xenoliths, Figs. 1, 2) within ignimbrites of the Upper Chegem Caldera. Fourteen minerals were discovered in xenolith no. 1; three in xenolith no. 3; one in xenolith no. 5; and three in xenolith no. 7 (Fig. 2, Table 1). In the recently discovered xenoliths no. 9 and 11 (Fig. 2), two potential new minerals were detected: a boron analog of galuskinite (Lazic *et al.* 2012) and a fluorine analog of rustumite (Gfeller *et al.* 2013). Minerals of the edgrewite-hydroxyledgrewite series, associated with fluorchegemite, have a very limited distribution. Up to now they had only been detected in two small samples from xenolith no. 1. Thus, it was surprising that hydroxyledgrewite is a rock-forming mineral in xenolith no. 11.

The F-analog of chegemite, named fluorchegemite, $Ca_7(SiO_4)_3(F,OH)_2$, was first discovered in 2008 within kumtyubeite zones (Galuskina *et al.* 2009), where it forms small inclusions in large kumtyubeite grains (Fig. 3, Table 2). The secondary minerals bultfonteinite, ettringite-thaumasite, garnets of the katoite-grossular series, hydrocalumite, afwillite, and hillebrandite are widespread in the kumtyubeite zones. The primary minerals in these zones are larnite, spurrite, lakargiite, srebrodolskite, perovskite, magnesioferrite, wadalite, and rondorfite (Galuskina *et al.* 2009).

During field work in 2009, relatively large grains of fluorchegemite, up to 0.2 mm in size, were detected (Fig. 4A, B; Table 2). Together with fluorchegemite the two new minerals edgrewite $Ca_9(SiO_4)_4F_2$ (IMA2011-058) and eltybyuite $Ca_{12}Fe^{3+}{}_{10}Si_4O_{32}Cl_6$ (IMA2011-022) were discovered in the same samples (Galuskin *et al.* 2012a, 2013). Calcium-humite minerals are confined to whitish strongly altered zones. The content of

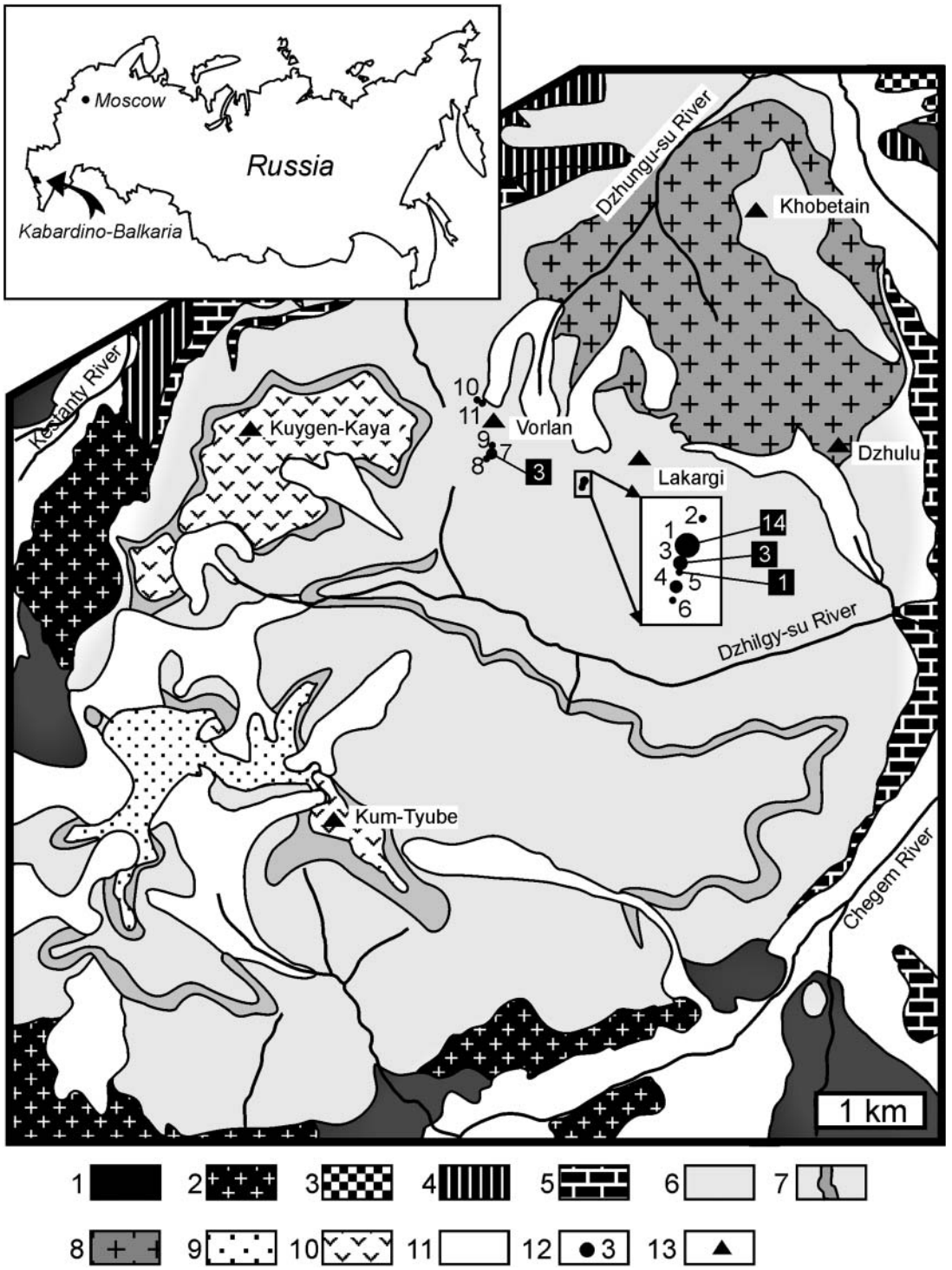
Moscow
Russia
Kabardino-Balkaria
Dzhungu-su River
Khobetain
Kestanty River
Kuygen-Kaya
Vorlan
Dzhulu
Lakargi
Dzhilgy-su River
Kum-Tyube
Chegem River
1 km
1
2
3
4
5
6
7
8
9
10
11
12
13

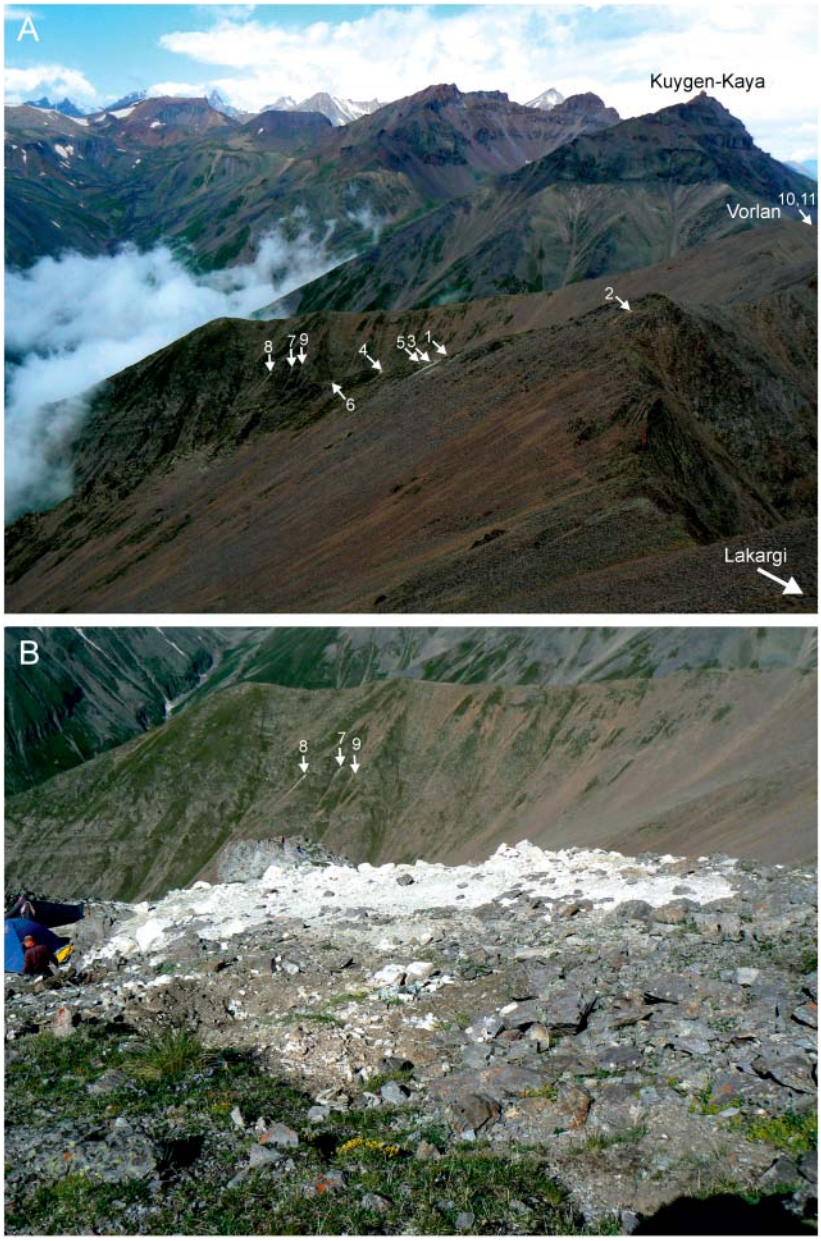

FIG. 2. (A) General view of the northwest part of the Upper Chegem Caldera; numbers indicate xenoliths and their positions. Xenoliths are distinguished on the ignimbrite background by a white color. (B) xenolith no. 1 in the foreground, type locality of fluorchegemite. The distance between xenoliths no. 1 and no. 7 is more than 1 km.

FIG. 1. Geological map of the Upper Chegem Caldera (after Gazeev *et al.* 2006 and Galuskin *et al.* 2009, simplified). The inset map shows the location of Kabardino-Balkaria. Legend: (1–5) Formations of different ages of the volcanic basement. 1,2 Structural zone of the Greater Caucasus Mountain Range: 1 Crystalline schist and gneiss; 2 Granite gneiss; 3 Permian conglomerate, sandstone and argillaceous slate; 4,5 Jurassic terrigenous carbonaceous formations; 4 Argillite, siltstone, and sandstone; 5 Limestone. (6–10) Neogene-Quaternary formations. 6 Rhyolite and rhyodacite ignimbrites; 7 Horizon of tuff and lavas in ignimbrites; 8 Granodiorite; 9 Glacial sediments of the Mindel Glaciation; 10 Post-Mindel Glaciation andesite lavas. (11) Quaternary glacial, alluvial, and proluvial sediments. (12) Location and number of the xenoliths. (13) Mountain peaks above 3000 m. White numbers in black squares correspond to discovered mineral species in specific xenoliths.

TABLE 1. MINERALS DISCOVERED IN LAKARGI LOCALITY, UPPER CHEGEM CALDERA, KABARDINO-BALKARIA, RUSSIA

	Mineral	Xenolith	IMA number	Formula		Group
1	lakargiite	1	IMA2007-014	$CaZrO_3$	Galuskin *et al.* 2008	perovskite
2	calcio-olivine	3	IMA07-B	γ -Ca_2SiO_4	Zadov *et al.* 2008	olivine
3	chegemite	1	IMA2008-038	$Ca_7(SiO_4)_3(OH)_2$	Galuskin *et al.* 2009	humite
4	kumtyubeite	1	IMA2008-045	$Ca_5(SiO_4)_2F_2$	Galuskina *et al.* 2009	humite
5	magnesioneptunite	5	IMA2009-009	$KNa_2Li(Mg, Fe)_2Ti_2Si_8O_{24}$	Zadov *et al.* 2011	neptunite
6	vorlanite	7	IMA2009-032	$CaU^{6+}O_4$	Galuskin *et al.* 2011a	uraninite
7	toturite	3	IMA2009-033	$Ca_3Sn_2Fe_2SiO_{12}$	Galuskina *et al.* 2010a	schorlomite
8	elbrusite	1	IMA2009-051	$Ca_3Zr_{1.5}U^{6+}{}_{0.5}Fe_3O_{12}$	Galuskina *et al.* 2010b	bitikleite
9	bitikleite	1	IMA2009-052	$Ca_3SnSbAl_3O_{12}$	Galuskina *et al.* 2010c	bitikleite
10	usturite	7	IMA2009-053	$Ca_3ZrSbFe_3O_{12}$	Galuskin *et al.* 2010c	bitikleite
11	megawite	3	IMA2009-090	$CaSnO_3$	Galuskin *et al.* 2011b	perovskite
12	pavlovskyite	1	IMA2010-063	$Ca_8(SiO_4)_2(Si_3O_{10})$	Galuskin *et al.* 2012a	
13	dzhuluite	1	IMA2010-064	$Ca_3SbSnFe^{3+}{}_3O_{12}$	Galuskina *et al.* 2013a	bitikleite
14	rusinovite	1	IMA2010-072	$Ca_{10}(Si_2O_7)_3Cl_2$	Galuskin *et al.* 2011c	
15	irinarassite	7	IMA2010-073	$Ca_3Sn_2SiAl_2O_{12}$	Galuskina *et al.* 2013b	schorlomite
16	eltyubyuite	1	IMA2011-022	$Ca_{12}Fe^{3+}{}_{10}Si_4O_{32}Cl_6$	Galuskin *et al.* 2013c	wadalite
17	aklimaite	1	IMA2011-050	$Ca_4[(Si_2O_5)(OH)_2](OH)_4{\cdot}5H_2O$	Zadov *et al.* 2012	
18	edgrewite	1	IMA2011-058	$Ca_9(SiO_4)_4F_2$	Galuskin *et al.* 2012b	humite
19	fluorchegemite	1	IMA2011-112	$Ca_7(SiO_4)_3F_2$	this volume	humite
20	hydroxyledgrewite	1	IMA2011-113	$Ca_9(SiO_4)_4(OH)_2$	Galuskin *et al.* 2012b	humite
21	chlorkyuygenite	1	IMA2012-046	$Ca_{12}Al_{14}O_{32}[(H_2O)_4Cl_2]$	Galuskin *et al.* 2014	mayenite

Ca-humite minerals is rather low in fresh rock fragments with weakly altered larnite grains and dark magnesioferrite crystals (Fig. 4A).

Acicular fluorchegemite crystals up to 0.1 mm in size are irregularly distributed in this rock, associated with relatively large edgrewite crystals (Fig. 4C). Calcium-humite minerals are strongly replaced by late hydrosilicate minerals. Larger acicular fluorchegemite crystals, up to 0.2 mm in size, form aggregates replacing larnite in lens-shaped assemblages (Fig. 4B). These crystals were studied for the description of the new mineral species.

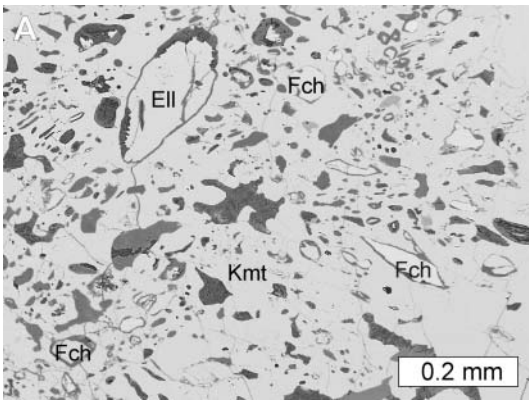

FIG. 3. Inclusions of fluorchegemite (Fch) and fluorellestadite (Ell) in kumtyubeite (Kmt).

Wadalite-eltyubyuite, rondorfite, lakargiite, and kerimasite are high temperature accessory and minor minerals, whereas the secondary minerals are bultfonteinite, killalaite, hillebrandite, afwillite, trabzonite, jennite, and others. Kerimasite associated with fluorchegemite and edgrewite (Fig. 4D) has an unusual composition (Table 3). Kerimasite forming late-stage zones on fine-grained aggregates of lakargiite displays increased U_2O_5 content up to 7 wt.% (Table 3, analysis 4). The rims of small crystals of kerimasite showed a ThO_2 content up to 4 wt.%, being the highest hitherto reported in natural garnet (Grew *et al.* 2013). We interpret zones with fluorchegemite and edgrewite as endoskarn developed after ignimbrite. The formation mechanism of lens-shaped Ca-humite aggregates and the crystal chemical peculiarity of uranium and thorium in kerimasite is treated in the Discussion section.

Fluorchegemite is colorless, and the streak is white. It forms irregular grains; in rare cases individual crystals have a rhombic cross-section. Twins are occasionally noted. The cleavage is imperfect on (010) and the fracture is irregular. Density could not be measured because of numerous inclusions of other minerals; the calculated density is 2.91 g cm^{-3}. The micro-hardness VHN (load

TABLE 2. CHEMICAL COMPOSITION OF Ca-HUMITES FROM ALTERED XENOLITHS FROM THE CAUCASIAN VOLCANITES

	Upper Chegem Caldera												Shadil-Khokh volcano					
	edgrewite zone			kumtyubeite zone						hydroxyledgrewite zone			larnite zone			spurrite zone		
	fluorchegemite			fluorchegemite			kumtyubeite			hydroxyledgrewite			fluorchegemite			kumtyubeite		
	mean 10	s.d.	range	mean 8	s.d.	range	mean 20	s.d.	range	mean 12	s.d.	range	mean 12	s.d.	range	mean 14	s.d.	range
wt.%																		
TiO_2	0.17	0.08	0.04–0.27	0.15	0.03	0.12–0.22	0.20	0.05	0.11–0.28	0.07	0.03	0.03–0.15	0.06	0.11	0–0.41	0.12	0.10	0.01–0.28
SiO_2	29.91	0.22	29.43–30.13	30.09	0.09	29.96–30.22	28.04	0.11	27.89–28.26	31.14	0.19	30.89–31.53	29.83	0.44	28.55–30.32	28.04	0.23	27.57–28.36
Al_2O_3	<0.02			<0.02			<0.02			<0.02			<0.03			0.06	0.07	0–0.29
CaO	65.65	0.20	65.31–66.01	66.15	0.22	65.67–66.33	66.16	0.19	65.78–66.62	65.63	0.30	65.11–66.29	65.44	0.32	64.92–66.17	65.90	0.44	65.15–66.52
MgO	0.04	0.01	0.03–0.05	<0.02			<0.02			<0.02			<0.02			<0.02		
MnO	<0.06			<0.06			<0.06	0.02	0–0.07	<0.06			<0.06			<0.06		
F	4.43	0.25	4.07–4.97	3.77	0.26	3.40–4.11	6.21	0.18	5.93–6.57	2.05	0.29	1.52–2.49	6.14	0.36	6.57–7.70	8.67	0.49	8.91–10.63
Cl	<0.06			<0.06			<0.06			<0.06			0.08	0.02	0.06–0.14	0.15	0.09	0.06–0.46
H_2O	0.90			1.24			1.25			1.39			0.08			0.08		
–O=F+Cl	1.88			1.60			2.63			0.86			2.60			3.86		
Total	99.22			99.80			99.23			99.41			99.06			99.16		
	Calculated on *n*(O+OH+F),* – *n* = 10, ** – *n* = 14 and *** – *n* = 18																	
Ca	7.01**			7.02**			5.01*			9.01***			7.02**			5.01*		
Mg	0.01																	
X	***7.02***			***7.02***			***5.01***			***9.01***			***7.02***			***5.01***		
Si	2.98			2.98			1.98			3.99			2.98			1.99		
Ti^{4+}	0.01			0.01			0.01			0.01			0.01			0.01		
Al																0.01		
Z	***2.99***			***2.99***			***1.99***			***4.00***			***2.99***			***2.01***		
Cl													0.01			0.02		
F	1.40			1.18			1.39			0.83			1.94			1.94		
OH	0.60			0.82			0.59			1.19			0.05			0.04		

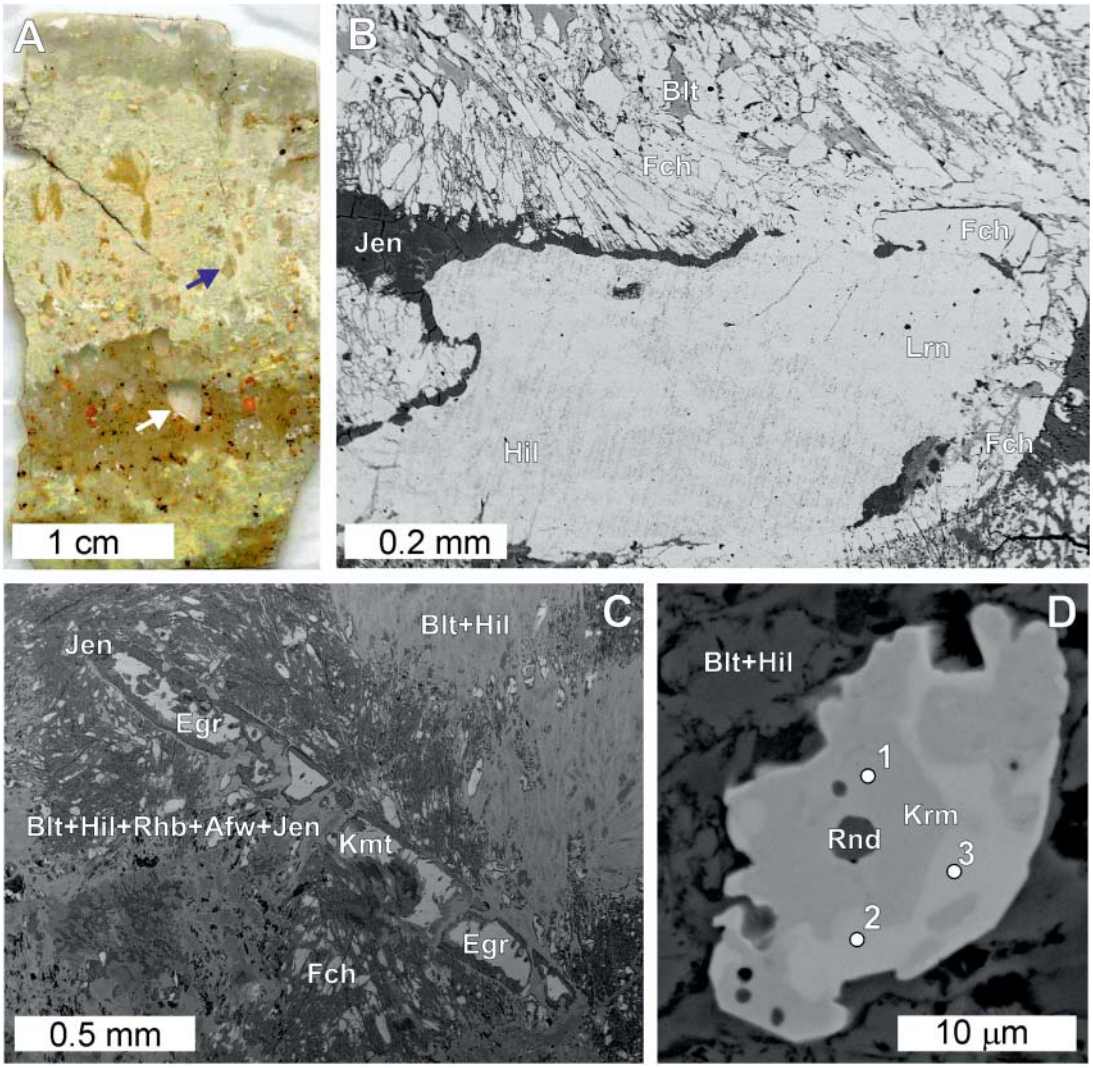

FIG. 4. (A) Polished specimen from an endoskarn zone. Brown zone: larnite zone with magnesioferrite (dark) is replaced by albescent zone containing fluorchegemite and edgrewite. The blue arrow indicates an altered larnite lens (its magnification is shown in Fig. 4B), whereas the white arrow indicates an unaltered larnite lens. Figures 4A–B were obtained with back-scattered electrons (BSE). (B) Fragment of larnite lens partially substituted by fluorchegemite. (C) Partially altered edgrewite crystal; the dark background is mainly composed of late hydrosilicate minerals and bultfonteinite with fluorchegmite. (D) Kerimasite crystal containing zones enriched in Th and U; analysis points are shown by numbers corresponding to those in Table 3. Fch – fluorchegemite, Lrn – larnite, Rhb – reinhardbraunsite, Kmt – kumtyubeite, Hil – hillebrandite, Blt – bultfonteinite, Jen – jennite, Edg – edgrewite, Krm – kerimasite, Rnd - rondorfite.

50 g) is: range 480–511 kg mm^{-2} (four measurements); mean 499(10) kg corresponds to the Mohs' scale of 5.5–6. Fluorchegemite is optically biaxial (–), α 1.610(2), β 1.6150(2), γ 1.619(2) (589 nm), $2V_z$(meas.) = 80(8)°, $2V_z$ (calc.) = 84°, birefringence 0.009, dispersion r > v, weak; orientation: $X = a$, $Y = b$, $Z = c$ (*Pbnm* setting), non-pleochroic. The Gladstone-Dale compatibility factor (Mandarino 1981) $1 - (K_p/K_c)$ = 0.00053 (excellent) was obtained using the empirical chemical formula (Table 2).

The composition of fluorchegemite is relatively homogeneous. The low Ti concentrations probably substitute for tetrahedral Si (Table 2). The chegemite $Ca_7(SiO_4)_3(OH)_2$ endmember component in the holotype specimen is about 30%. In similar zones in a different part of xenolith no. 1, OH-dominant chegemite is

TABLE 3. CHEMICAL COMPOSITION OF Th-RICH KERIMASITE FROM THE EDGREWITE ZONE

wt.%	1	2	3	4
U_2O_5	2.06	3.82	3.32	7.13
Nb_2O_5	0.17	0.71	0.47	0.41
Sb_2O_5	<0.1	2.92	2.90	<0.1
SiO_2	6.12	3.21	2.95	5.47
TiO_2	3.95	3.03	2.78	4.45
ZrO_2	35.38	28.05	28.56	30.34
SnO_2	2.66	3.99	3.59	1.42
HfO_2	0.64	1.06	1.13	0.58
ThO_2	0.13	2.90	4.02	0.20
Al_2O_3	4.84	4.80	4.83	4.58
Sc_2O_3	0.26	0.20	0.41	0.45
Fe_2O_3	17.37	20.65	20.42	18.83
La_2O_3	0.09	<0.08	<0.08	0.13
Ce_2O_3	0.19	0.29	0.34	0.34
CaO	26.40	24.40	23.93	25.68
Total	100.26	100.01	99.62	99.99
	calculated on 12O *pfu*			
Ca	2.991	2.922	2.897	2.980
Th	0.003	0.074	0.103	0.005
La	0.003			0.005
Ce	0.008	0.012	0.014	0.013
X	**3.005**	**3.007**	**3.014**	**3.003**
Zr	1.824	1.528	1.573	1.603
U^{5+}	0.047	0.092	0.081	0.167
Nb^{5+}	0.008	0.036	0.024	0.020
Sn	0.112	0.178	0.161	0.061
Sb^{5+}		0.121	0.121	
Hf	0.019	0.034	0.036	0.018
Sc	0.024	0.019	0.040	0.042
Ti^{4+}				0.089
Y	**2.035**	**2.008**	**2.038**	**2.000**
Fe^{3+}	1.382	1.737	1.736	1.535
Al	0.603	0.633	0.643	0.584
Si	0.647	0.359	0.333	0.592
Ti^{4+}	0.314	0.255	0.236	0.274
Z	**2.947**	**2.983**	**2.949**	**2.985**

observed, but minerals of the edgrewite-hydroxyledgrewite series are absent. Fluorchegemite in kumtyubeite inclusions contains about 40% of the chegemite endmember (Table 2).

Minerals belonging to the fluorchegemite-chegemite series are widespread in xenoliths from the Upper Chegem Caldera; usually, compositions close to the boundary between F-dominant and OH-dominant members occur (usually, with OH > F).

Raman spectra of fluorchegemite, chegemite from the Upper Chegem Caldera, and chegemite from South Osetia (see below) are shown in Figure 5. In the Raman spectrum of fluorchegemite the following characteristic bands are distinguished (cm^{-1}, strong bands are underlined): 258, 297, 410 (ν_2), 422 (ν_2), 560 (ν_4), 817 (ν_1), 843 (ν_1), 922 (ν_3), 3539 (ν_{OH}), 3548 (ν_{OH}), 3552 (ν_{OH}). The Raman spectra of fluorchegemite and chegemite are similar but differ in the number of bands in the OH region (Fig. 5; Galuskin *et al.* 2009). All bands in the Raman spectra of Ca-humite minerals can be divided into four groups: (1) bands in the region below 350 cm^{-1} correspond to vibrations of CaO_6 octahedra; (2) bands in the region 350–750 cm^{-1} correspond to the bending vibrations of SiO_4 tetrahedra; (3) bands in the region 750–1000 cm^{-1} are interpreted as stretching vibrations of SiO_4; (4) bands in the region 3400–3600 cm^{-1} are related to the OH-stretching vibrations

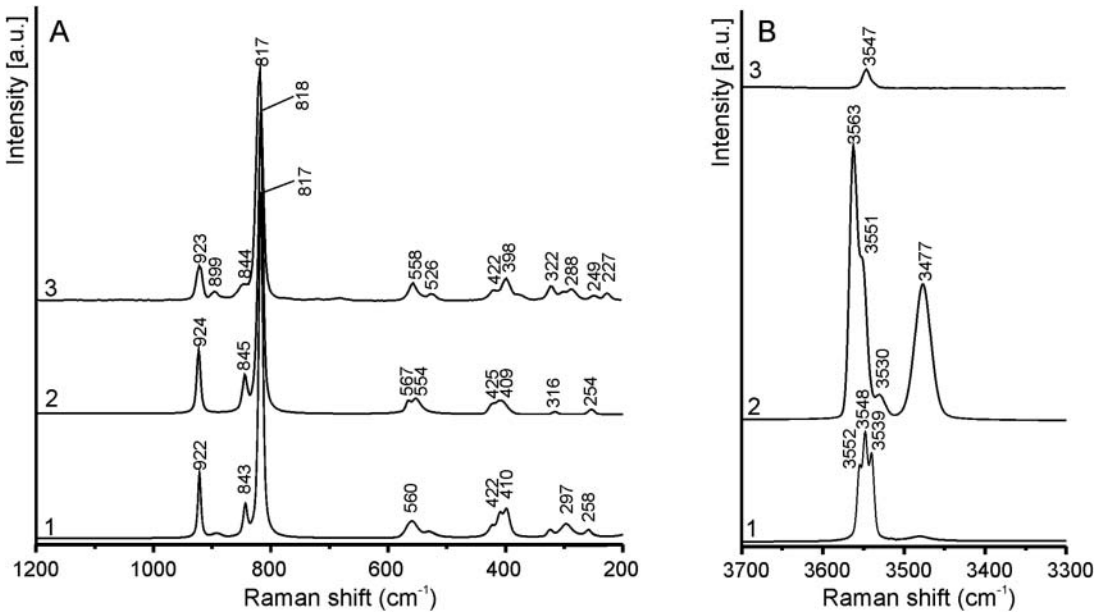

FIG. 5. Raman spectra of fluorchegemite (1) and chegemite (2) from the Upper Chegem Caldera and fluorchegemite (3) from the Shadil-Khokh volcano. (A) 1200–200 cm^{-1} region, (B) 3700–3000 cm^{-1} region.

(Galuskin *et al.* 2009, 2012a, Galuskina *et al.* 2009). Fluorine-dominant minerals of the Ca-humite series (kumtyubeite, fluorchegemite, edgrewite) often show band splitting at about 3550 cm^{-1}, whereas hydroxyl analogues (reinhardbraunsite, chegemite, hydroxyledgrewite) are characterized by two well-resolved main bands at about 3560 and 3450 cm^{-1} (Fig. 5).

An unpolarized FTIR reflection spectrum of fluorchegemite (Fig. 6) shows the following bands (the strong active bands are underlined): 756 cm^{-1}, 795 cm^{-1}, 805 cm^{-1}, 821 cm^{-1}, 844 cm^{-1}, 866 cm^{-1}, 889 cm^{-1}, 914 cm^{-1}, 934 cm^{-1}, 962 cm^{-1}, 991 cm^{-1}, 1031 cm^{-1}, 1102 cm^{-1}, 3552 cm^{-1}. The FTIR spectrum of fluorchegemite is similar to those shown by chegemite and the other members of the humite group. Strong FTIR bands in the fluorchegemite spectrum are related to asymmetric stretching vibrations in $(SiO_4)^{4-}$ tetrahedra (Frost 2007, Galuskin *et al.* 2009). In both the Raman and the FTIR spectra of fluorchegemite only one weak OH-characteristic band at 3552 cm^{-1} was recorded.

An X-ray powder pattern was calculated from the atomic coordinates of the crystal structure using PowderCell for Windows version 2.4 (Kraus & Nolze 1996). Such data are by far superior to data obtained from an impure mineral concentrate (Table 4).

Crystal Structure of Fluorchegemite

The crystal structure of fluorchegemite corresponds to that of chegemite (Galuskin *et al.* 2009) and is compatible with the humite structure type (Ribbe & Gibbs 1971). X-ray single-crystal data collection and refinement details for fluorchegemite are summarized in Tables 5 through 8. The framework of the chegemite-type structure is composed of zigzag chains of four symmetry-independent Ca-octahedra linked by two types of isolated Si-tetrahedra (Galuskin *et al.* 2009). Average Ca–O distances in fluorchegemite vary between 2.35 Å (Ca4) and 2.40 Å (Ca2). These distances are very similar to those in reinhardbraunsite $Ca_5(SiO_4)_2(OH,F)_2$ and calcio-olivine γ-Ca_2SiO_4 (Kirfel *et al.* 1983, Gobechiya *et al.* 2008).

A projection of a polyhedral structure model of chegemite along [100] is indistinguishable from a corresponding drawing for humite (Ribbe & Gibbs 1971, Galuskin *et al.* 2009) with the only obvious difference being that the volume of fluorchegemite is 34% greater than that of humite due to the difference in octahedral ionic radii, 0.72 Å for Mg *versus* 1.00 Å for Ca (Shannon 1976). A special feature of the chegemite structure is the strongly anisotropic smearing of O8 related to positional and chemical disorder. In fluorchegemite F8/O8 is up to 70% occupied by F and up to 30% occupied by O. The F8 position centers a triangular plane with 2 × Ca4 and 1 × Ca3 at the corners. The disorder, represented by anisotropic displacement parameters (Table 7), is most pronounced perpendicular to the triangular plane.

Structurally investigated chegemite (Galuskin *et al.* 2009) had the composition $Ca_7(SiO_4)_3[(OH)_{1.5}F_{0.5}]$,

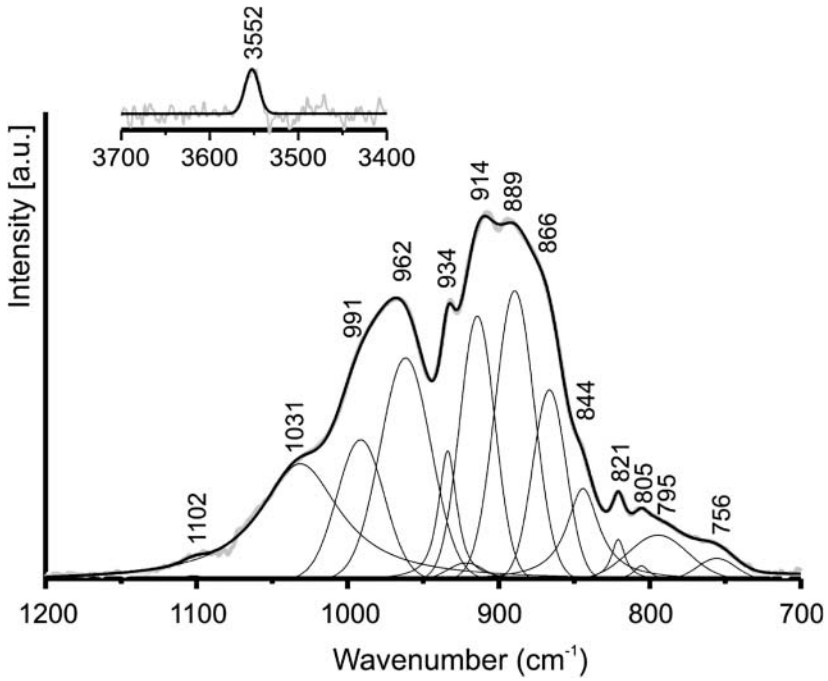

FIG. 6. Unpolarized reflected FTIR spectrum of fluorchegemite.

while fluorchegemite used for structure refinement in this study was an F-dominant [(OH),F] solid-solution member, $Ca_7(SiO_4)_3[F_{1.2}(OH)_{0.8}]$. From this point of view it is not surprising that the corresponding structure refinements yielded very similar results. However, according to Shannon (1976), F^- has a slightly smaller ionic radius than $(OH)^-$. This difference is also obvious from the Ca4–F8/O8 distances of 2.296(1) and 2.304(1) Å in fluorchegemite compared to Ca4–O8/F8 of 2.307(1) and 2.321(1) Å in chegemite. To a lesser degree, the difference can also be observed for the distance Ca3–F8/O8 of 2.314(1) Å in fluorchegemite *versus* 2.318(1) in chegemite. As seen in Figure 7, shortened Ca4–F8/O8 and Ca3–F8/O8 distances will especially influence the *a* and *c* cell dimensions, which are for fluorchegemite [*a* 5.0620(1), *b* 11.3917(2), *c* 23.5180(3) Å] significantly smaller than for chegemite [*a* 5.0696(1), *b* 11.3955(1), *c* 23.5571(3) Å]. These differences also show up in the unit-cell volume of 1356.16(4) $Å^3$ for fluorchegemite compared to 1360.91(4) $Å^3$ for chegemite.

In the system of hydrogen bonds in chegemite $Ca_7(SiO_4)_3(OH)_2$ (Galuskin *et al.* 2009), O8 acts simultaneously as donor and acceptor of a hydrogen bond (Fig. 7). In the case of an intermediate composition between fluorchegemite and chegemite, splitting of O8 into two sites (O8 and F8) is observed. Comparable features have been observed for other members of the Ca-humite series. The chegemite structure with O/F = 0.72/0.28 was refined with split O8 and F8 positions, leading to the scheme of hydrogen bonds: O8–H1…O8 = 2.847 Å, confirmed by a Raman band near 3480 cm^{-1}; the O8–H1…F8 = 3.229 Å and O8–H2…O7 = 3.200 Å interactions are responsible for the the additional bands at 3540–3560 cm^{-1} (Figs. 5 and 7, Galuskin *et al.* 2009). In fluorchegemite the main hydrogen bond is O8–H1…F8 (Fig. 7), yielding a characteristic Raman spectrum with very low intensity of the band at 3480 cm^{-1} and reduced intensity of the bands at 3540–3560 cm^{-1} (Fig. 5).

DISCUSSION

Formation mechanism of fine grained Ca-humite lenses

We have already discussed the formation conditions of Ca-humite minerals in altered xenoliths within ignimbrites of the Upper Chegem Caldera. The metamorphism reached sanidinite facies (larnite subfacies) characterized by 750–900 °C under low-pressure conditions (Galuskina *et al.* 2009, Galuskin *et al.* 2009, 2012a,b).

Reinhardbraunsite-kumtyubeite and, more rarely, chegemite-fluorchegemite are rock-forming minerals in exoskarn zones in carbonate-silicate xenoliths. Reinhardbraunsite-kumtyubeite replace spurrite zones according to $Ca_5(SiO_4)_2CO_3 + H_2O + F_2 = Ca_5(SiO_4)_2(F,OH)_2 + CO_2$ (Galuskina *et al.* 2009). Chegemite-fluorchegemite layers probably formed from galuskinite

TABLE 4. CALCULATED POWDER DIFFRACTION PATTERN FOR FLUORCHEGEMITE (Cu$K\alpha$ = 1.5406 Å, BRAGG-BRENTANO GEOMETRY, FIXED SLIT, NO ANOMALOUS DISPERSION)

h	*k*	*l*	*d*	I_{rel}	*h*	*k*	*l*	*d*	I_{rel}
0	0	2	11.759	5	2	1	5	2.187	1
0	0	4	5.88	3	2	2	4	2.15	5
0	2	0	5.696	4	1	1	10	2.096	7
0	2	1	5.536	12	1	5	1	2.07	2
0	2	2	5.126	16	1	5	2	2.046	1
1	1	0	4.626	1	1	5	3	2.008	5
1	1	2	4.305	1	1	2	10	1.997	4
1	0	3	4.253	12	1	0	11	1.97	1
0	2	4	4.091	22	1	5	4	1.959	3
1	1	3	3.984	14	1	1	11	1.941	7
0	0	6	3.92	7	2	0	8	1.918	3
1	2	1	3.736	12	2	2	7	1.905	90
1	1	4	3.636	52	2	4	0	1.892	31
1	2	2	3.602	1	1	3	10	1.86	8
1	0	5	3.446	3	2	4	3	1.839	15
1	2	3	3.408	2	1	5	6	1.836	5
1	1	5	3.298	6	0	6	4	1.807	21
1	2	4	3.182	3	1	1	12	1.805	2
1	3	0	3.038	45	1	6	1	1.773	1
1	3	1	3.013	57	1	5	7	1.767	10
1	1	6	2.991	56	2	4	5	1.755	1
0	0	8	2.94	8	1	3	11	1.748	12
1	3	2	2.941	4	0	2	13	1.724	6
0	2	7	2.894	28	0	4	11	1.71	14
0	4	0	2.848	7	2	4	6	1.704	6
1	3	3	2.832	51	1	6	4	1.702	1
1	1	7	2.718	63	1	5	8	1.697	3
1	3	4	2.699	46	0	0	14	1.68	28
0	4	3	2.677	17	3	1	0	1.669	2
1	3	5	2.552	9	3	1	1	1.665	3
2	0	0	2.531	100	0	6	7	1.653	36
1	2	7	2.512	29	3	0	3	1.65	1
1	1	8	2.481	20	1	3	12	1.647	3
1	4	0	2.482	19	3	1	3	1.633	5
2	1	0	2.471	8	2	5	4	1.627	1
2	1	1	2.457	2	1	4	11	1.62	2
0	4	5	2.436	1	3	2	1	1.614	2
2	1	2	2.418	1	3	1	4	1.606	4
1	3	6	2.401	7	1	3	13	1.554	5
2	1	3	2.357	4	1	7	0	1.549	11
0	4	6	2.304	5	1	7	1	1.546	7
2	1	4	2.278	5	3	3	0	1.542	3

according to $Ca_7(SiO_4)_3CO_3 + H_2O + F_2 = Ca_7(SiO_4)_3(OH,F)_2 + CO_2$ (Galuskin *et al.* 2012a).

More frequently, fluorchegemite-chegemite assemble aggregates are represented by elongated lenses in the endoskarn (Figs. 4A, B). These aggregates contain larnite relics and minute kumtyubeite-reinhardbraunsite grains. This lens type, with the elongated axis oriented subperpendicular to the ignimbrite contact (or skarn zoning), is characteristic for endoskarn zones of all known xenoliths from this locality (Fig. 8A, B). At the intimate contact with ignimbrite such lens-shaped aggregates consist of larnite with wollastonite and rankinite (Figs. 8A, C-E), and more rarely with cuspidine or rusinovite (Galuskin *et al.* 2011a, 2012b). In the newly found xenolith no. 11, corresponding larnite lenses are most often substituted by rusinovite, $Ca_{10}(Si_2O_7)_3Cl_2$, rustumite, $Ca_{10}(Si_2O_7)_2(SiO_4)(OH,F)_2Cl_2$, and cuspidine, $Ca_4(Si_2O_7)F_2$ (Fig. 8G), whereas larnite lenses more

TABLE 5. PARAMETERS FOR X-RAY DATA COLLECTION AND CRYSTAL-STRUCTURE REFINEMENT

Crystal data	fluorchegemite
Unit cell dimensions (Å)	a = 5.0620(1) b = 11.3917(2) c = 23.5180(3) α = β = γ = 90°
Space group	*Pbnm* (No. 62)
Volume (Å^3)	1356.16(4)
Z	4
Chemical formula	$Ca_7(SiO_4)_3[F_{1.2}(OH)_{0.8}]$
Crystal shape	prismatic
Crystal size (μm)	40 × 60 × 120
Diffractometer	APEX II BRUKER SMART
X-ray radiation	Mo$K\alpha$ (0.71073 Å)
X-ray power	50 kV, 30 mA
Monochromator	Graphite
Temperature	293(2)
Detector to sample distance	6 cm
Measurement method	Phi and Omega scans
Time per frame	10 sec
Max. θ°-range for Data collection	36.36
Index ranges	$-8 \le h \le 7$ $-15 \le k \le 17$ $-37 \le l \le 32$
No. of measured reflections	11802
No. of unique reflections	3016
No. of observed reflections (I > 2σ (I))	2272
Refinement of the structure	
No. of parameters used in refinement	119
Rint	0.0238
$R\sigma$	0.0229
$R1$, I > 2σ(I)	0.0235
$R1$ all Data	0.0398
w$R2$ on (F^2)	0.0509
GooF	1.030
Δρ min (–e. Å^{-3})	0.47 close to Si1
Δρ max (e. Å^{-3})	0.50 close to O2

distant to the contact are replaced by hydroxyledgrewite (Fig. 8F). This type of occurrence is the second finding of hydroxyledgrewite in nature (Table 1). Xenolith no. 11 is located more than 2 km from xenolith no. 1, which is the type locality for edgrewite and hydroxyledgrewite (Figs. 1, 2; Galuskin *et al.* 2012a). The characteristic contours of the lenses formed after quartz phenocrysts in the ignimbrite. The formation mechanism is discussed below (Fig. 9).

Ignimbrite of the Upper Chegem Caldera consists of up to 60–80% porous glass responsible for high permeability of gases and fluids. This porous matrix enables diffusion of Ca cations from the carbonate xenolith towards the ignimbrite. In the case of the biggest xenolith, no. 1, the thickness of the endoskarn zone may exceed 1 m. Quartz crystals extending into the skarn boundary are transformed to elongated lenses consisting of Ca-silicate minerals (Fig. 9A). The process of quartz replacement takes place under non-equilibrium conditions of fast Si diffusion towards the xenolith, but relatively slow Ca diffusion towards the ignimbrite. As a result, a lens-like contour forms around original quartz in the endoskarn. At the intimate contact of the ignimbrite with the carbonate-silicate xenolith (Fig. 8C, D), these lenses are composed of fine-grained and fibrous Ca-silicate minerals (wollastonite, rankinite, pavlovskyite, larnite). A succession of metasomatic micro-zones (up to 1–2 μm) forming on quartz at the skarn front (Galuskin *et al.* 2012b) shows the sequence quartz – wollastonite – rankinite – pavlovskyite – larnite (Fig. 9B). We consider this as an important observation, because when distinguishing skarn zonation at a macroscopic scale, micro-zonation is often neglected, although micro-zones act as membranes and have a significant bearing on the general processes of diffusion and metasomatism.

In the early stage of skarn formation, the presence of chlorine leads to crystallization of abundant wadalite and rondorfite in the endo- and exoskarn zones of altered xenoliths of the Upper Chegem Caldera (Galuskin *et al.* 2009, Galuskina *et al.* 2009). The high chlorine activity is responsible for replacement of wollastonite, rankinite, and larnite at the contact zones (Figs. 8G, 9B) by rusinovite, $Ca_{10}(Si_2O_7)Cl_2$, and rustumite, $Ca_{10}(Si_2O_7)(SiO_4)Cl_2(OH)_2$. At a later stage of skarn formation the fluorine activity increases, leading to replacement of larnite by cuspidine and Ca-humite minerals at the intimate contact with the ignimbrite (Figs. 4A, B, 8A, B, 9B, C). The decisive parameter determining formation of Ca-silicate minerals is the Ca/Si ratio in the local environment, which increases from ignimbrite (Si >> Ca) towards the spurrite zone (Ca/Si = 2.5/1) and towards marble relics of the xenolith core (Ca>>Si). Lens-shaped aggregates of larnite are substituted by Ca-humite minerals, reflecting the local Ca/Si ratio in the rock (Fig. 9C). Volcanic gases and fluids, enriched in F(+Cl) and H_2O, promoted the crystallization of several Ca-humite minerals and play an important role in the alteration of primary spurrite and larnite-bearing skarns. Fluorine-dominant Ca-humite minerals formed at higher temperature at an early stage and were subsequently replaced by OH-dominant Ca-humite minerals.

A second occurrence of fluorchegemite in a xenolith from the Shadil-Khokh volcano, Southern Ossetia

A relatively large altered xenolith of carbonate-silicate rock, more than 2 m in size, was discovered in

TABLE 6. ATOMIC COORDINATES AND EQUIVALENT ISOTROPIC DISPLACEMENT PARAMETERS (Å^2) FOR FLUORCHEGEMITE

Site	Occ.	*x/a*	*y/b*	*z/c*	U_{eq}
Ca1	1	0.50365(5)	0.37780(2)	0.176429(10)	0.00869(6)
Ca2	1	–0.50760(8)	0.65766(3)	0.2500	0.00771(7)
Ca3	1	–0.00413(5)	0.59334(2)	0.110841(11)	0.00813(6)
Ca4	1	0.50734(5)	0.36123(2)	0.027438(11)	0.00868(6)
Si1	1	–0.07139(10)	0.47082(5)	0.2500	0.00626(10)
Si2	1	0.07483(8)	0.27951(3)	0.106683(15)	0.00647(7)
O1	1	–0.7508(3)	0.46992(12)	0.2500	0.0090(3)
O2	1	–0.2975(3)	0.83816(11)	0.2500	0.0082(2)
O3	1	–0.20235(19)	0.53659(8)	0.19460(4)	0.00856(17)
O4	1	0.75398(19)	0.27928(9)	0.10536(4)	0.00931(19)
O5	1	0.2041(2)	0.41197(8)	0.10424(4)	0.00888(18)
O6	1	0.29625(19)	0.71711(8)	0.16344(4)	0.00857(17)
O7	1	0.2068(2)	0.21047(8)	0.05223(4)	0.00894(18)
F8	0.7	0.7533(2)	0.53016(9)	0.03330(4)	0.0204(2)
O8	0.3	0.7533(2)	0.53016(9)	0.03330(4)	0.0204(2)
H1	0.3	0.923(10)	0.505(8)	0.015(3)	0.050

F8: occupancy 0.7, O1, H1: occupancy 0.3

plagiodacite lava on the northwest flank of the Shadil-Khokh volcano (~30 Ma in age), Kel volcanic plateau, Great Caucasus Mountain Range, Southern Ossetia. The mineral association of the xenolith, *i.e.*, spurrite, larnite, gehlenite, merwinite, bredigite, rondorfite, srebrodolskite, is typical for pyrometamorphic rocks of the sanidinite facies (Gazeev *et al.* 2012). Some portions of the xenolith are well zoned. The contact of larnite-merwinite-melilite-rondorfite-wadalite with spurrite-fluorellestadite zones is shown in Figure 10A. In the spurrite zone bright pink spherules of kumtyubeite, blue spots of fluorellestadite, and yellow spots of a potential new mineral, the Cl-analog of jasmundite, are noted. In an intermediate grey zone fluorellestadite and larnite prevail. In the white marginal part of the spurrite zone, aggregates of acicular galuskinite crystals are associated with larnite and, more rarely, patches of acicular, colorless fluorchegemite are observed (Fig. 10B). Fluorchegemite and kumtyubeite from the Shadil-Khokh volcano contain very low end-member contents (~2%) of their hydroxyl analogs: chegemite and reinhardbraunsite, respectively. The Raman spectrum of fluorchegemite from the Shadil-Khokh volcano is comparable to the one of fluorchegemite from the Upper Chegem Caldera (Fig. 5). The only difference in the former is the very low intensity of the band at 3540 cm^{-1}, reflecting the low OH content.

TABLE 7. ANISOTROPIC DISPLACEMENT PARAMETERS (Å^2) FOR FLUORCHEGEMITE

Site	U_{11}	U_{22}	U_{33}	U_{23}	U_{13}	U_{12}
Ca1	0.00810(11)	0.01086(12)	0.00712(11)	–0.00188(8)	–0.00107(8)	–0.00066(10)
Ca2	0.00877(16)	0.00696(15)	0.00740(14)	0.000	0.000	0.00029(13)
Ca3	0.00938(12)	0.00732(11)	0.00769(11)	0.00038(8)	0.00027(9)	–0.00063(9)
Ca4	0.00978(12)	0.00921(12)	0.00704(11)	0.00028(8)	0.00074(9)	–0.00032(10)
Si1	0.0059(2)	0.0068(2)	0.0060(2)	0.000	0.000	–0.00004(18)
Si2	0.00640(16)	0.00709(16)	0.00592(15)	0.00005(12)	–0.00019(12)	0.00020(13)
O1	0.0073(6)	0.0102(6)	0.0095(6)	0.000	0.000	0.0006(5)
O2	0.0088(6)	0.0073(6)	0.0085(6)	0.000	0.000	0.0002(5)
O3	0.0089(4)	0.0104(4)	0.0063(4)	0.0018(3)	–0.0006(3)	0.0004(4)
O4	0.0065(4)	0.0109(4)	0.0106(4)	0.0003(4)	–0.0002(3)	–0.0003(3)
O5	0.0100(4)	0.0073(4)	0.0093(4)	0.0000(3)	–0.0008(3)	0.0006(4)
O6	0.0090(4)	0.0098(4)	0.0069(4)	0.0013(3)	0.0001(3)	0.0000(4)
O7	0.0097(4)	0.0099(4)	0.0072(4)	–0.0011(3)	0.0004(3)	0.0001(4)
F8	0.0239(5)	0.0151(5)	0.0223(5)	0.0010(4)	–0.0112(4)	–0.0013(4)
O8	0.0239(5)	0.0151(5)	0.0223(5)	0.0010(4)	–0.0112(4)	–0.0013(4)

TABLE 8. SELECTED INTERATOMIC DISTANCES (Å) FOR FLUORCHEGEMITE

Atom	–Atom	distance	Atom	–Atom	distance
Ca1	–O5	2.309(1)	Ca4	–O7	2.280(1)
	–O2	2.326(1)		–O8/F8	2.296(1)
	–O4	2.379(1)		–O8/F8	2.304(1)
	–O3	2.381(1)		–O7	2.367(1)
	–O6	2.398(1)		–O4	2.406(1)
	–O1	2.399(1)		–O5	2.440(1)
	Mean	2.365		Mean	2.349
Ca2	–O2	2.315(1)	Si1	–O1	1.623(1)
	–O6	2.364(1)×2		–O3	1.642(1)×2
	–O3	2.447(1)×2		–O2	1.651(1)
	–O1	2.468(1)		Mean	1.640
	Mean	2.401	Si2	–O4	1.624(1)
Ca3	–O3	2.304(1)		–O7	1.644(1)
	–O8/F8	2.314(1)		–O5	1.646(1)
	–O5	2.325(1)		–O6	1.647(1)
	–O6	2.415(1)		Mean	1.640
	–O7	2.438(1)	O8	–H1	0.995(19)
	–O4	2.470(1)			
	Mean	2.378			

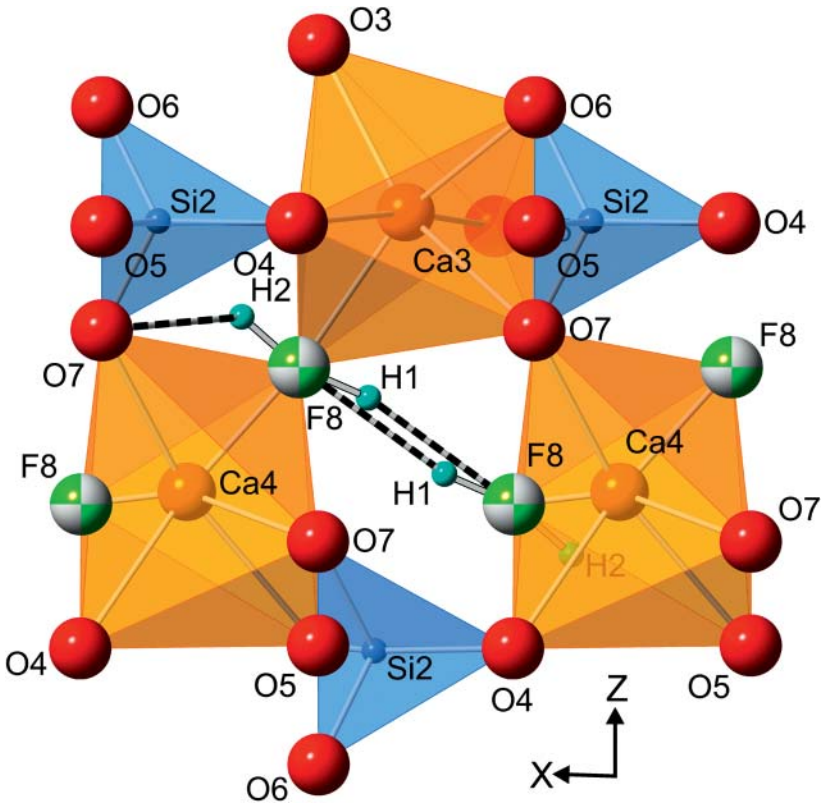

FIG. 7. Scheme of hydrogen bonds in minerals of the chegemite-fluorchegemite series.

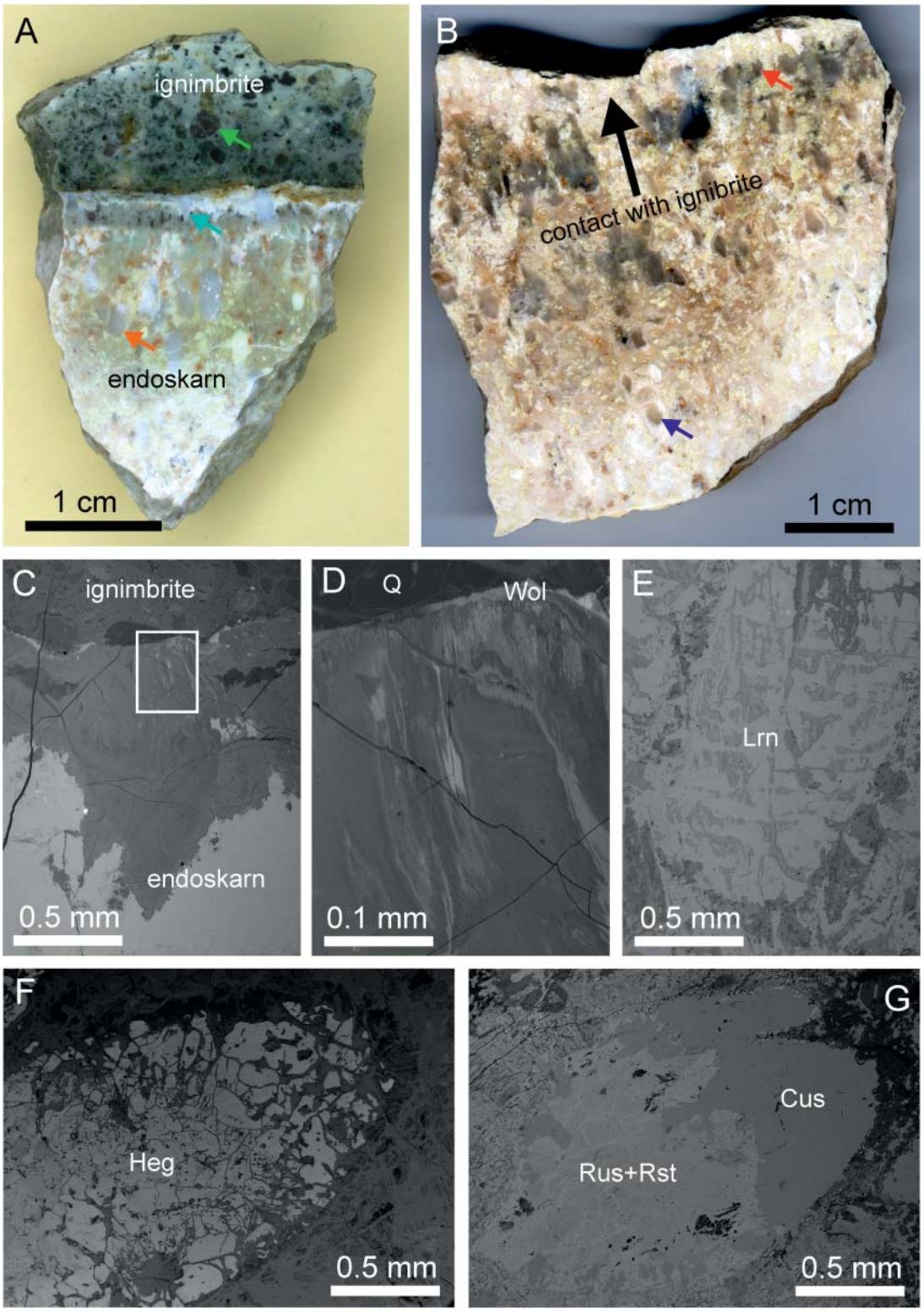
A
ignimbrite
endoskarn
1 cm
B
contact with ignibrite
1 cm
C
ignimbrite
endoskarn
0.5 mm
D
Q
Wol
0.1 mm
E
Lrn
0.5 mm
F
Heg
0.5 mm
G
Cus
Rus+Rst
0.5 mm

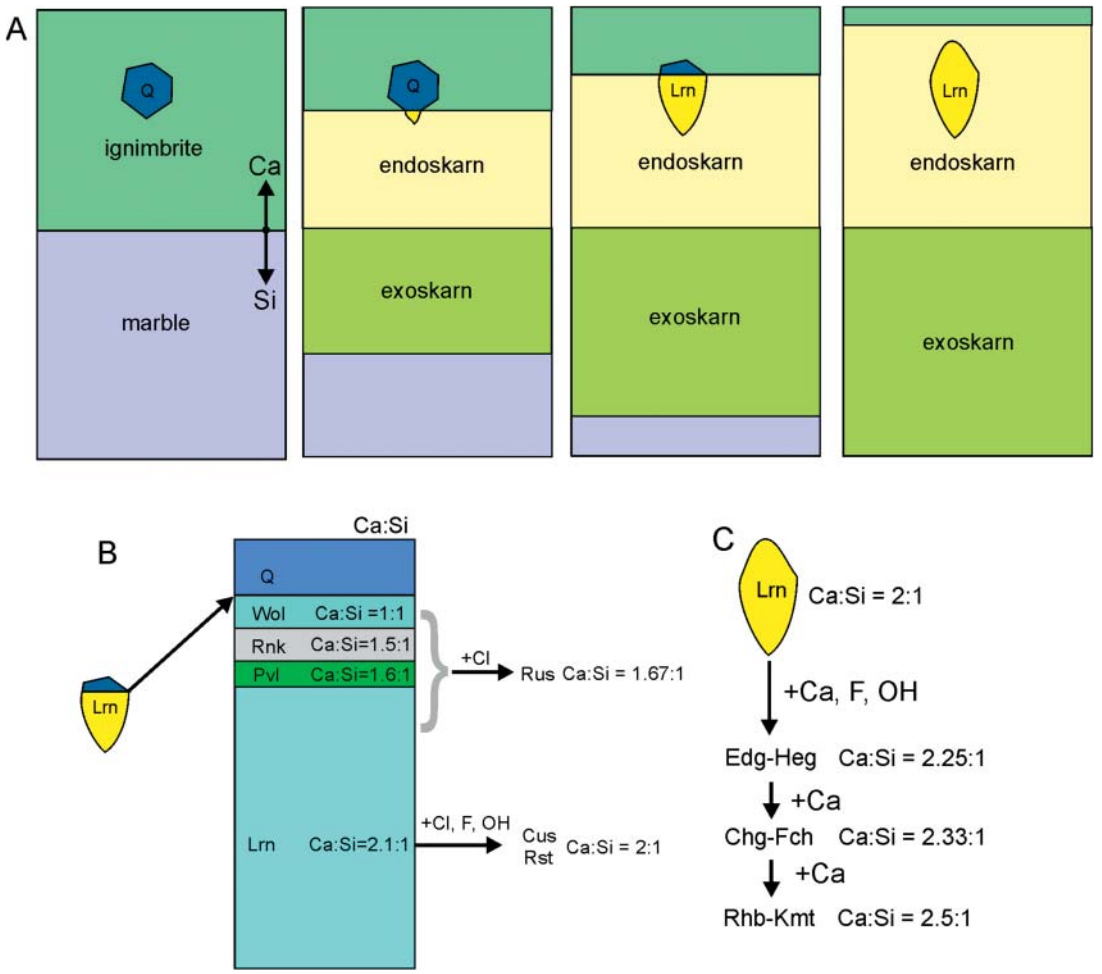

FIG. 9. Sketch of larnite lens formation in endoskarn. (A) Simplified mechanism of ignimbrite quartz phenocrysts replacement leading to formation of larnite lenses with their elongated axis oriented subperpendicular to the boundary of replacement. (B) Metasomatic micro-zones between quartz and larnite. (C) Sequence of replacement of larnite by Ca-humite minerals defined by increasing Ca activity in the endoskarn.

Thorian kerimasite

Kerimasite crystals in endoskarn associated with fluorchegemite and edgrewite are products of Ca-metasomatism of accessory zircon in the ignimbrite. Zircon occasionally forms intergrowths with thorite, allanite-Ce, or minerals of the apatite supergroup. The unusual garnet-supergroup mineral

FIG. 8. (A) Contact of ignimbrite and endoskarn. Green arrow: quartz in ignimbrite; blue arrow: lens-like heterogeneous aggregate of Ca-silicate minerals at the boundary between endoskarn and slightly altered ignimbrite (the selected portion is magnified in Figs. 8C and D); orange arrow: larnite lens with rankinite relics (magnified in Fig. 8E). (B) Endoskarn (xenolith no. 11) intensively replaced by secondary hydrosilicate minerals and enriched in hydroxyledgrewite forming granular lens-like aggregates. Arrows show fragments magnified in Figure 8G (red arrow) and Figure 8F (blue arrow). (C) Heterogeneous lens-like aggregate formed after quartz phenocryst in ignimbrite; a small part on the ignimbrite side is still SiO_2. Calcium-silicates (wollastonite, rankinite, and larnite) forming lens-like aggregates are partially hydrated. The outlined area is magnified in Figure 8D. Figures 8C–G were produced with back scattered electrons (BSE). (D) Wollastonite micro-zone decorating the contact with quartz. (E) Larnite lens-like aggregate containing rankinite relics (grey). (F) Hydroxyledgrewite lens with larnite relics. (G) Rare type of lens-like aggregates of rusinovite (grey) replaced by rustumite (light). The tip of the lens is filled by cuspidine. Wol – wollastonite, Lrn – larnite, Heg – hydroxyledgrewite, Rus – rusinovite, Rst – rustumite, Cus – cuspidine.

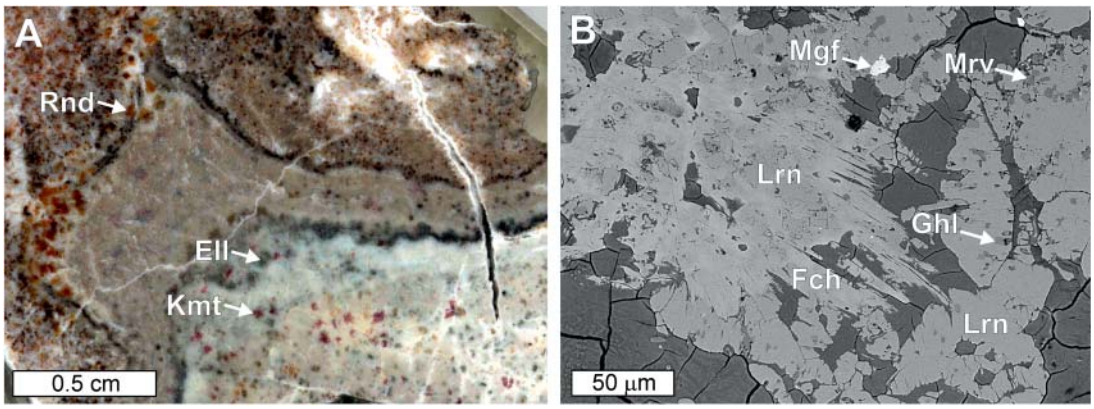

FIG. 10. (A) Fragment of altered xenolith from the Shadil-Khoch volcanites. (B) Aggregates of fluorchegemite in association with larnite (back-scattered electron picture). Fch – fluorchegemite, Lrn – larnite, Kmt – kumtyubeite, Ell – fluorellestadite, Mgf – magnesioferrite, Rnd – rondorfite, Ghl – gehlenite, Mrv – mervinite.

kerimasite with maximum ThO_2 content of 4 wt.% (Table 3) has the formula: $(Ca_{2.897}Th_{0.103}Ce_{0.014})_{\Sigma 3.014}(Zr_{1.573}Sn_{0.161}Sb^{5+}_{0.121}U^{5+}_{0.081}Sc_{0.040}Nb^{5+}_{0.024})_{\Sigma 2.038}(Fe^{3+}_{1.736}Al_{0.643}Si_{0.333}Ti_{0.236})_{\Sigma 2.949}O_{12}$, requiring explanation. This garnet shows very low Si content (<0.5 *apfu*), but its assignment to the schorlomite group as kerimasite was based on the dominant valence rule (Hatert & Burke 2008): Si+Ti > 0.5 *apfu* and Si > Ti at the Z site. The low Si content of this kerimasite leads to a significant component of Si-free garnet endmembers of the bitikleite group, such as $\{Ca_{2.5}Th_{0.5}\}[Zr_2](R^{3+}_3)O_{12}$, $\{Ca_3\}[ZrSb^{5+}](R^{3+}_3)O_{12}$, and $\{Ca_3\}[ZrU^{5+}](R^{3+}_3)O_{12}$ (Galuskina *et al.* 2010b, Grew *et al.* 2013). The accepted crystal chemical formula of the uranian garnet elbrusite is $\{Ca_3\}[Zr_{1.5}U^{6+}_{0.5}](R^{3+}_3)O_{12}$ (Grew *et al.* 2013). However, our recent studies of elbrusite from the Caucasus and Jordan showed that uranium in the garnet structure occurs as U^{5+}, thus the crystal chemical formula of elbrusite should be revised to $\{Ca_3\}[ZrU^{5+}](R^{3+}_3)O_{12}$ (Galuskina *et al.* 2014b). If we will apply the standard elbrusite formula, a significant part of the iron has to be calculated as Fe^{2+}, leading to an unrealistic yafsoanite-like endmember $\{Ca_3\}[U^{6+}_2](Fe^{2+}_3)O_{12}$ (Grew *et al.* 2013). There are two reasons why that yasfoanite-like endmember is considered unrealistic: (1) the relatively large Fe^{2+} occurs tetrahedrally coordinated, and (2) uranian garnets in pyrometamorphic rocks from the Caucasus and Jordan formed at high oxidizing conditions reflected in the composition of associated ferric minerals with only Fe^{3+}. Kerimasite associated with fluorchegemite and edgrewite in endoskarn zones of the Upper Chegem shows the highest Th concentration among natural garnet, corresponding to a 20% $\{Ca_{2.5}Th_{0.5}\}[Zr_2](R^{3+}_3)O_{12}$ endmember.

ACKNOWLEDGMENTS

The authors are thankful to Associate Editor Dr. Henrik Friis and Reviewers Dr. Ulf Hålenius and Dr. Cristian Biagioni for useful and constructive comments. This work was partially supported by research project No. UMO-2013/11/B/ST10/00272 of the National Science Centre of Poland.

REFERENCES

BOGATIKOV, O.A., GURBANOV, A.G., KOVALENKO, V.I., KORONOVSKY, N.V., LIPMAN, P., & TSVETKOV, A.A. (1992) The Upper Chegem caldera complex in Northern Caucasus. *International Geology Review* **34(2)**, 131–147.

BORSUK, A.M. (1979) *Mesozoic and Cenozoic magmatic formations of Great Caucasus.* Nauka, Moscow, Russia, 1–299 (in Russian).

DEER, W.A., HOWIE, R.A., & ZUSSMAN, J. (1982) *Rock-forming Minerals, Orthosilicates* **1A**, 2nd Edition. Longman, London, England, 936 pp.

FROST, R.L., PALMER, S.J., BOUZAID, J.M., & REDDY, B.J. (2007) A Raman spectroscopic study of humite minerals. *Journal of Raman Spectroscopy* **38**, 68–77.

GALUSKIN, E.V., GAZEEV, V.M., ARMBRUSTER, T., ZADOV, A.E., GALUSKINA, I.O., PERTSEV, N.N., DZIERŻANOWSKI, P., KADIYSKI, M., GURBANOV, A.G., WRZALIK, R., & WINIARSKI, A. (2008) Lakargiite, $CaZrO_3$: a new mineral of the perovskite group from the North Caucasus, Kabardino-Balkaria, Russia. *American Mineralogist* **93**, 1903–1910.

GALUSKIN, E.V., GAZEEV, V.M., LAZIC, B., ARMBRUSTER, T., GALUSKINA, I.O., ZADOV, A.E., PERTSEV, N.N., WRZALIK,

R., DZIERŻANOWSKI, P., GURBANOV, A.G., & BZOWSKA, G. (2009) Chegemite, $Ca_7(SiO_4)_3(OH)_2$—a new calcium mineral of the humite-group from the Northern Caucasus, Kabardino-Balkaria, Russia. *European Journal of Mineralogy* **21**, 1045–1059.

GALUSKIN, E.V., GALUSKINA, I.O., LAZIC, B., ARMBRUSTER, T., ZADOV, A.E., KRZYKAWSKI, T., BANASIK, K., GAZEEV, V. M., & PERTSEV, N.N. (2011a) Rusinovite $Ca_{10}(Si_2O_7)_3Cl_2$ – a new skarn mineral from the Upper Chegem caldera, Kabardino-Balkaria, Northern Caucasus, Russia. *European Journal of Mineralogy* **23**, 837–844.

GALUSKIN, E.V., ARMBRUSTER, T., GALUSKINA, I.O., LAZIC, B., WINIARSKI, A., GAZEEV, V.M., DZIERŻANOWSKI, P., ZADOV, A.E., PERTSEV, N.N., WRZALIK, R., GURBANOV, A.G., & JANECZEK, J. (2011b) Vorlanite $(CaU^{6+})O_4$—a new mineral from the Upper Chegem caldera, Kabardino-Balkaria, Northern Caucasus, Russia. *American Mineralogist* **96**, 188–196.

GALUSKIN, E.V., LAZIC, B., ARMBRUSTER, T., GALUSKINA, I.O., PERTSEV, N.N., GAZEEV, V.M., WŁODYKA, R., DULSKI, M., DZIERŻANOWSKI, P., ZADOV, A.E., & DUBROVINSKY, L.S. (2012a) Edgrewite $Ca_9(SiO_4)_4F_2$-hydroxyledgrewite $Ca_9(SiO_4)_4(OH)_2$, a new series of calcium humite-group minerals from altered xenoliths in the ignimbrite of Upper Chegem caldera, Northern Caucasus, Kabardino-Balkaria, Russia. *American Mineralogist* **97**, 1998–2006.

GALUSKIN, E.V., GFELLER, F., SAVELYEVA, V.B., ARMBRUSTER, T., LAZIC, B., GALUSKINA, I.O., TÖBBENS, D.M., ZADOV, A. E., DZIERŻANOWSKI, P., PERTSEV, N.N., & GAZEEV, V.M. (2012b) Pavlovskyite $Ca_8(SiO_4)_2(Si_3O_{10})$—a new mineral of altered silicate-carbonate xenoliths from the two Russian type localities: Birkhin massif, Baikal Lake area and Upper Chegem caldera, North Caucasus. *American Mineralogist* **97**, 503–512.

GALUSKIN, E.V., GALUSKINA, I.O., BAILAU, R., PRUSIK, K., GAZEEV, V.M., ZADOV, A.E., PERTSEV, N.N., JEŻAK, L., GURBANOV, A.G., & DUBROVINSKY, L. (2013) Eltyubyuite, $Ca_{12}Fe^{3+}{}_{10}Si_4O_{32}Cl_6$ - the Fe^{3+} analogue of wadalite: A new mineral from the Northern Caucasus, Kabardino-Balkaria, Russia. *European Journal of Mineralogy* **25**, 221–229.

GALUSKIN, E.V., GALUSKINA, I.O., KUSZ, J., ARMBRUSTER, T., MARZEC, K.M., DZIERŻANOWSKI, P., & MURASHKO, M. (2014) Vapnikite Ca_3UO_6 - A new double-perovskite mineral from pyrometamorphic larnite rocks of the Jabel Harmun, Palestinian Autonomy, Israel. *Mineralogical Magazine* **78(3)**, 571–581.

GALUSKINA, I.O., LAZIC, B., ARMBRUSTER, T., GALUSKIN, E.V., GAZEEV, V.M., ZADOV, A.E., PERTSEV, N.N., JEŻAK, E., WRZALIK, R., & GURBANOV, A.G. (2009) Kumtyubeite $Ca_5(SiO_4)_2F_2$—a new calcium mineral of the humite group from Northern Caucasus, Kabardino-Balkaria, Russia. *American Mineralogist* **94**, 1361–1370.

GALUSKINA, I.O., GALUSKIN, E.V., ARMBRUSTER, T., LAZIC, B., DZIERŻANOWSKI, P., GAZEEV, V.M., PRUSIK, K., PERTSEV, N. N., WINIARSKI, A., ZADOV, A.E., WRZALIK, R., & GURBANOV, A.G. (2010a) Bitikleite-(SnAl) and bitikleite-(ZrFe)—new garnets from xenoliths of the Upper Chegem volcanic structure, Kabardino-Balkaria, Northern Caucasus, Russia. *American Mineralogist* **95**, 959–967.

GALUSKINA, I.O., GALUSKIN, E.V., ARMBRUSTER, T., LAZIC, B., KUSZ, J., DZIERŻANOWSKI, P., GAZEEV, V.M., PERTSEV, N. N., PRUSIK, K., ZADOV, A.E., WINIARSKI, A., WRZALIK, R., & GURBANOV, A.G. (2010b) Elbrusite-(Zr)—a new uranian garnet from the Upper Chegem caldera, Kabardino-Balkaria, Northern Caucasus, Russia. *American Mineralogist* **95**, 1172–1181.

GALUSKINA, I.O., VAPNIK, YE., LAZIC, B., ARMBRUSTER, T., MURASHKO, M., & GALUSKIN, E.V. (2014a) Harmunite $CaFe_2O_4$ – a new mineral from the Jabel Harmun, West Bank, Palestinian Autonomy, Israel. *American Mineralogist* **99**, 965–975.

GALUSKINA, I., GALUSKIN, E., UTSUNOMIYA, S., NAKAMATSU, Y., MURASHKO, M., & VAPNIK, Y. (2014b) Uranian garnet from pyrometamorphic rocks of the Hatrurim Complex, Jordan. Problem of crystal chemical formula of elbrusite. *Abstracts of 21st General Meeting of IMA*, South Africa, 2014, 378 p.

GAZEEV, V.M., ZADOV, A.E., GURBANOV, A.G., PERTSEV, N.N., MOKHOV, A.V., & DOKUCHAEV, A.Y. (2006) Rare minerals from Verkhniechegemskaya caldera (in xenoliths of skarned limestone). *Vestnik Vladikavkazskogo Nauchnogo Centra* **6**, 18–27 (in Russian).

GAZEEV, V.M., GURBANOVA, O.A., ZADOV, A.E., GURBANOV, A. G., & LEKSIN, A.B. (2012) Mineralogy of skarned carbonate xenoliths from Shadil-khokh volcano (Kelski Vulcan area of Great Caucasian Range). *Vestnik Vladikavkazskogo Nauchnogo Centra* **2**, 18–27 (in Russian).

GAZIS, C.A., LANPHERE, M., & TAYLOR, H.P. (1995) $^{40}Ar/^{39}Ar$ and $^{18}O/^{16}O$ studies of the Chegem ash-flow caldera and the Eldjurta Granite: Cooling of two Pliocene igneous bodies in the Greater Caucasus Mountains, Russia. *Earth and Planetary Science Letters* **134**, 377–391.

GFELLER, F., ARMBRUSTER, T., GALUSKIN, E.V., GALUSKINA, I. O., LAZIC, B., SAVELYEVA, V.B., ZADOV, A.E., DZIERŻANOWSKI, P., & GAZEEV, V.M. (2013) Crystal chemistry and hydrogen bonding of rustumite $Ca_{10}(Si_2O_7)_2(SiO_4)(OH)_2Cl_2$ with variable OH, Cl, F. *American Mineralogist* **98**, 493–500.

GOBECHIYA, E.R., YAMNOVA, N.A., ZADOV, A.E., & GAZEEV, V.M. (2008) Calcio-olivine γ-Ca_2SiO_4: I. Rietveld refinement of the crystal structure. *Crystallography Reports* **53(3)**, 404–408.

GRAPES, R. (2011) *Pyrometamorphism.* Springer, London, England, 365 p.

GREW, E.S., LOCOCK, A.J., MILLS, S.J., GALUSKINA, I.O., GALUSKIN, E.V., & HÅLENIUS, U. (2013) IMA Report: Nomenclature of the garnet supergroup. *American Mineralogist* **98**, 785–811.

HAMM, H.-M. & HENTSCHEL, G. (1983) Reinhardbraunsite, $Ca_5(SiO_4)_2(OH,F)_2$ equivalent of synthetic "calcio-chondrodite". *Neues Jahrbuch für Mineralogie, Monatshefte*, 119–129.

HATERT, F. & BURKE, E.A.J. (2008) The IMA–CNMNC dominant-constituent rule revisited and extended. *Canadian Mineralogist* **46**, 717–728.

HRŠELOVÁ, P., CEMPÍREK, J., HOUZAR, S., & SEJKORA, J. (2013) S,F,Cl-rich mineral assemblages from burned spoil heaps in the Rosice-Oslavany coalfield, Czech republic. *Canadian Mineralogist* **51**, 171–188.

KANTAUTAS, A., PALUBINSKAITÉ, D., & VAICKELIONIS, G. (2006) Synthesis and hardening of fluoralinite cement. *Materials Science-Poland* **24**, 385–393.

KIRFEL, A., HAMM, H.M., & WILL, G. (1983) The crystal structure of reinhardbraunsite, $Ca_5(SiO_4)_2(OH,F)_2$, a new mineral of the calcio-chondrodite type. *Tschermaks Mineralogische und Petrographische Mitteilungen* **31**, 137–150.

KRAUS, W. & NOLZE, G. (1996) POWDER CELL – a program for the representation and manipulation of crystal structures and calculation of resulting X-ray powder patterns. *Journal of Applied Crystallography* **29**, 301–303.

LAZIC, B., ARMBRUSTER, T., SAVELYEVA, V.B., ZADOV, A.E., PERTSEV, N.N., & DZIERŻANOWSKI, P. (2011) Galuskinite, $Ca_7(SiO_4)_3(CO_3)$, a new skarn mineral from the Birkhin gabbro massif, Eastern Siberia, Russia. *Mineralogical Magazine* **75**, 2631–2548.

LAZIC, B., ARMBRUSTER, T., GALUSKINA, I.O., ZIELIŃSKI, G., DZIERŻANOWSKI, P., & GALUSKIN, E.V. (2012) B- and As-bearing galuskinite and B-analog of galuskinite from Upper Chegem caldera, Northern Caucasus, Russia. *European Mineralogical Conference* **1**, EMC2012-55.

LIPMAN, P.W., BOGATIKOV, O.A., TSVETKOV, A.A., GAZIS, A. G., GURBANOV, A.G., HON, K., KORONOVSKY, N.V., KOVALENKO, V.I., & MARCHEV, P. (1993) 2.8 Ma ash-flow caldera at Chegem River in the northern Caucasus Mountains (Russia): Contemporaneous granites, and associated ore deposits. *Journal of Volcanology and Geothermal Research* **57**, 85–124.

MANDARINO, J.A. (1981) The Gladstone – Dale relationship: Part IV. The compatibility concept and its application. *Canadian Mineralogist* **19**, 441–450.

RIBBE, P.H. (1982) The humite series and Mn-analogs. *In* Orthosilicates (P.H. Ribbe, ed.). *Reviews in Mineralogy* **5**, 231–274.

RIBBE, P.H. & GIBBS, G.V. (1971) Crystal structure of the humite minerals: III. Mg/Fe ordering in humite and its relation to other ferromagnesian silicates. *American Mineralogist* **56**, 1155–1173.

SHANNON, R.D. (1976) Revised effective ionic radii and systematic studies of interatomic distances in halides and chalcogenides. *Acta Crystallographica* **A32**, 751–767.

SHARYGIN, V.V. (2011) Lakargiite and minerals of the perovskite-brownmillerite series in metacarbonate rocks from Donetsk burned dumps. *Proceedings of the Donetsk National Technical University of Mining Geology* **15**, 113–123.

SHELDRICK, G.M. (2008) A short history of SHELX. *Acta Crystallographica* **A64**, 112–122.

SURESH, K., MURTHY, K.V.R., POORNACHANDRA RAO, N.V., & SUBBA RAO, B. (2011) Synthesis and photoluminescence tudy of $Ca_3Si_3O_8F_2$, $Ca_5Si_2O_8F_2$and $Ca_7Si_3O_{12}F_2$ doped with Ce, Eu and Tb containing fluorine. *International Journal of Luminescence and Applications* **1**, 52–55.

TAYLOR, H.F.W. (1997) *Cement chemistry*. Academic Press, London, England, 465 pp.

THOMPSON, J.B. (1978) Biopyriboles and polysomatic series. *American Mineralogist* **63**, 239–249.

Received October 28, 2014, revised manuscript accepted March 18, 2015.